Table of Contents

1 Introduction

A linear polymer, or macromolecule, is a long molecule formed by monomers joined in a sequence by covalent bonds. The structural properties of macromolecule depends on the system state. In good solvent, there is excluded volume effect and polymer is in denaturated, or unfolded, regime. Globular, or collapsed, phase corresponds to polymer immersed in poor solvent. In the critical point, the phase space is divided into two regions corresponding to open and globular states of polymer [1].

Coarse-grained models of macromolecules are widely used for macromolecular modeling. In these models, polymers are represented using subunits which are formed by groups of atoms instead of individual atoms (see Chap.1 in Ref.[2]). Such models neglect chemical details. As coarse-grained models decrease the number of degrees of freedom, it is convenient approach to simulate systems to obtain statistical properties.

The simplest model of polymer is classical homopolymer model which is represented by interacting (also known as collapsing) self-avoiding walk (SAW). This is well-studied model, including cases for different lattices (see Ref.[1, 3]). Self-avoiding walks allows to include excluded volume effects for polymers in good solvent. Van der Waals type attraction is modeled via including the nearest neighbor monomer attraction. Critical phenomena take place in the infinite systems in second order phase transition which is defined as a singularity of free-energy function (see Chap.3 in Ref [4]).

In homopolymer model, all monomers are the same. The polymers with different types of subunits are called heteropolymers. The simplest heteropolymer model is Hydrophobic-polar (HP) model of protein [5]. It assumes that the sequence of monomers types are fixed. This model was introduced to approximate the folding process of protein and mostly used for development algorithms to find minimum energy states (for example, [6, 7]). This model also was used to explore conformations space of proteins [8]. We studied the case of dynamical HP model where sequence of monomers and geometry structure are not fixed [9]. Computational results do not contradict the assumption that dynamical HP model and an interacting homopolymer have the similar behavior in phase transition point and they are in the same universality class.

To represent the ferromagnetic properties of material, the Ising model was introduced. The 2D square-lattice Ising model is the simplest example of system which undergoes a phase transition between ordered states. To study magnetic polymers, Garel et.al introduced the Ising model on self-avoiding walks [10] and studied it for 2D and 3D lattices [10, 11]. Recently, this model was studied [12, 13]. Computational results show that the system has second-order transition in 2D case and first-order transition on 3D lattice.

Classical XY model on 2D square lattice has a topological order, which was proposed theoretically and named Kosterlitz-Thouless (KT) phase transition [14]. After, classical 2D was studied numerically using Monte-Carlo methods [15, 16].

In this work, we continue to study magnetic polymer. We study XY model on SAWs for 2D and 3D lattices in lack of an external field. Part of this work including computational results for cubic lattice is submitted for Russian Supercomputing Days [17].

The rest of the paper is organized as follows. In Section 2 we describe XY model on SAWs. Next, we discuss Monte-Carlo algorithms and present the method we implement in section 3.This is followed by results of numerical simulations in Section 4. We conclude with the summary of our work.

2 Models

2.1 XY model on self-avoiding walks (SAWs)

A molecular conformation of the length N is represented by a self-avoiding walk (SAW) on a regular lattice with $N-1$ edges and N nodes. Each ith node represents a spin-like variable s_i which is associated with angle $\theta_i \in [-\pi;\pi]$. Figure 2.1 illustrates the model on the square lattice.

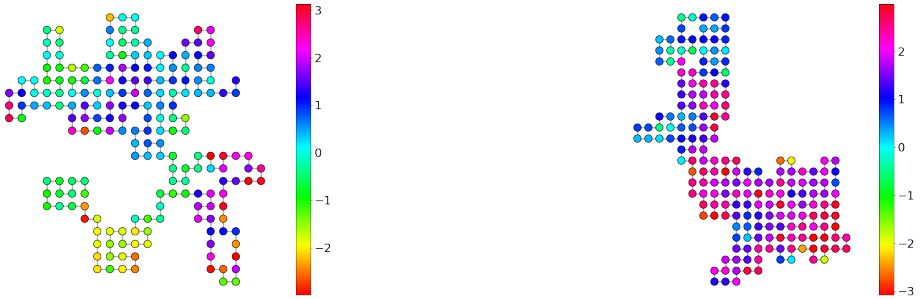

Figure 2.1: Example states of the chain $N = 200$ obtained using simulation at $J = 1.41$ on the square lattice. The color represents angle variable θ_i.

The Hamiltonian for sequence of spins s and conformation u is defined as the sum over all non-repeating neighbor pairs $\langle i,j\rangle$th in conformation:

$$H(u,s) = -J\sum_{\langle i,j\rangle} cos(\theta_i - \theta_j) - h\sum_i cos(\theta_i) \tag{2.1}$$

In our work, we focus on the system in lack of an external field: $h = 0$. Without loss of generality, we assume that $\beta = \frac{1}{kT} = 1$, where k is Boltzmann's constant, T is temperature.

Let U_N be a set of all SAW conformations of N monomers. The partition function for the chain of the length N is the sum over all SAW conformations of N monomers and the integral over all spin space:

$$Z(J) = \sum_{u\in U_N}\int_{-\pi}^{\pi}\frac{1}{(2\pi)^N}d\theta_1 d\theta_2 \ldots d\theta_N e^{J\cos(\theta_1-\theta_2)}e^{J\cos(\theta_2-\theta_3)}\ldots e^{J\cos(\theta_{N-1}-\theta_N)} \tag{2.2}$$

The mean magnetization is defined as a vector:

$$\langle\vec{m}\rangle = \frac{1}{N}\left\langle(\sum_{i=1}^{N}cos\theta_i, \sum_{i=1}^{N}sin\theta_i)\right\rangle \tag{2.3}$$

The second moment of magnetization is a square of the norm:

$$\langle m^2\rangle = \frac{1}{N^2}\left\langle(\sum_{i=1}^{N}cos\theta_i)^2 + (\sum_{i=1}^{N}sin\theta_i)^2\right\rangle \tag{2.4}$$

From measurements of the average magnetization per spin $\langle m \rangle(J)$, we can obtain the value of the magnetic cumulant (Binder parameters) of fourth order [18], which is helpful to study magnetic phase transition:

$$U_4(J) = 1 - \frac{\langle m^4 \rangle}{3\langle m^2 \rangle^2} \tag{2.5}$$

The Binder parameter could be used to determine the order of magnetic parameters [19]. At some continuous phase transition, the Binder ratio transitions approaches a step function as the system size is increased. The Binder ratio has a divergent feature at the step if the system has the first order transition.

2.1.1 Case without interaction (J=0)

Consider the case when no interaction which could be close to classical 1-dimensional XY-chain. In case of open boundary conditions, the partition function for the chain of the length N has following form:

$$Z(J) = \int_{-\pi}^{\pi} \frac{1}{(2\pi)^N} d\theta_1 d\theta_2 \dots d\theta_N e^{Jcos(\theta_1 - \theta_2)} e^{Jcos(\theta_2 - \theta_3)} \dots e^{Jcos(\theta_{N-1} - \theta_N)} \tag{2.6}$$

In case $J = 0$ (high-temperature regime), all states have equal probabilities:

$$Z(0) = \int_{-\pi}^{\pi} (\frac{1}{2\pi})^N d\theta_1 d\theta_2 \dots d\theta_N \tag{2.7}$$

To calculate the exact value of $\langle m^2 \rangle(J = 0)$ we use following results:

$$\int_{-\pi}^{\pi} \frac{1}{2\pi} sin^2\theta d\theta = \int_{-\pi}^{\pi} \frac{1}{2\pi} cos^2\theta d\theta = \frac{1}{2}$$

$$\int_{-\pi}^{\pi} \frac{1}{2\pi} sin\theta d\theta = \int_{-\pi}^{\pi} \frac{1}{2\pi} cos\theta d\theta = 0$$

After some calculation, only integration results for N times $sin^2\theta_i$ and N times $cos^2\theta_i$ survive:

$$\langle m^2 \rangle(J = 0) = \frac{1}{N^2} \int_{-\pi}^{\pi} (\frac{1}{2\pi})^N \left((\sum_{i=1}^{N} cos\theta_i)^2 + (\sum_{i=1}^{N} sin\theta_i)^2 \right) d\theta_1 d\theta_2 \dots d\theta_N = \frac{1}{N^2} (\frac{1}{2}N + \frac{1}{2}N) = \frac{1}{N} \tag{2.8}$$

Next, to calculate $\langle m^4 \rangle(J = 0)$ we use following facts:

$$\langle m^4 \rangle(J = 0) = \frac{1}{N^4} \int_{-\pi}^{\pi} (\frac{1}{2\pi})^N \left((\sum_{i=1}^{N} cos\theta_i)^2 + (\sum_{i=1}^{N} sin\theta_i)^2 \right)^2 d\theta_1 d\theta_2 \dots d\theta_N$$

$$\left((\sum_{i=1}^{N} cos\theta_i)^2 + (\sum_{i=1}^{N} sin\theta_i)^2 \right)^2 = (\sum_{i=1}^{N} cos\theta_i)^4 + (\sum_{i=1}^{N} sin\theta_i)^4 + 2(\sum_{i=1}^{N} cos\theta_i)^2 (\sum_{i=1}^{N} sin\theta_i)^2$$

$\int_{-\pi}^{\pi} \frac{1}{2\pi} sin^4\theta d\theta = \int_{-\pi}^{\pi} \frac{1}{2\pi} cos^4\theta d\theta = \frac{3}{8}$ (We have N times $sin^4\theta_i$-term and N times $cos^4\theta_i$-term what results in $2 \times \frac{3}{8} \times N$).

$\int_{-\pi}^{\pi}\frac{1}{2\pi}\int_{-\pi}^{\pi}\frac{1}{2\pi}sin^2\theta_i sin^2\theta_j d\theta_i d\theta_j = \int_{-\pi}^{\pi}\frac{1}{2\pi}\int_{-\pi}^{\pi}\frac{1}{2\pi}cos^2\theta_i cos^2\theta_j d\theta_i d\theta_j = \frac{1}{4}$ (We have $6N(N-1)\frac{1}{2}$ times *sin*-term and $6N(N-1)\frac{1}{2}$ times *cos*-term what results in $6\times\frac{1}{4}\times N(N-1)$).

$\int_{-\pi}^{\pi}\frac{1}{2\pi}sin^2\theta cos^2\theta d\theta = \frac{1}{8}$ (We have this term $2N$ times what results in $2\times\frac{1}{8}\times N$).

$\int_{-\pi}^{\pi}\frac{1}{2\pi}\int_{-\pi}^{\pi}\frac{1}{2\pi}cos^2\theta_i sin^2\theta_j d\theta_i d\theta_j = \frac{1}{4}$ (We have $2N(N-1)\frac{1}{2}$ times what results in $2\times\frac{1}{4}\times N(N-1)$).

All other terms with odd power of sin of cos function equals zero after integration over period.

$$\langle m^4\rangle(J=0) = \frac{1}{N^4}\left(2\times\frac{3}{8}\times N + 6\times\frac{1}{4}\times N(N-1) + 2\times\frac{1}{8}\times N + 2\times\frac{1}{4}\times N(N-1)\right) = \frac{2N-1}{N^3}$$

$$U_4(J=0) = 1 - \frac{\frac{2N-1}{N^3}}{3\frac{1}{N^2}} = 1 - \frac{2N-1}{3N} = \frac{1}{3} + \frac{1}{3N} \tag{2.9}$$

In classical Ising model, $U_4 \to 0$ as $J \to 0$. In our work, we use the common definition for Binder cumulant. Consequently, the lower limiting value in disordered state is $U_4 = \frac{1}{3}$.

2.2 Structural properties

To study structural phase transition, we use the mean square end-to-end distance (radius) of self-avoiding-walks which is defined as the sum over all configurations:

$$\langle R_N^2\rangle = \frac{1}{Z_N}\sum_{|u|=N}|u|^2 e^{-H(s,u)}, \tag{2.10}$$

where $|u|$ is the Euclidean distance between the endpoints of conformation u, and Z_N is partition function in the canonical assemble (2.6). We call it "mean radius" for brevity. As $N \to \infty$, the mean radius of SAWs is believed to scale as

$$\langle R_N^2\rangle \sim N^{2\nu}. \tag{2.11}$$

Here ν is a critical exponent, which is model-dependent. For thermodynamic limit $N \to \infty$, ν is believed to have the form of a step function of interaction energy J. For finite systems, this effect is rounded [3].

We define the scaling function for two chain lengths N_1, N_2:

$$\langle R_{N_1}^2\rangle \sim N_1^{2\nu}; \langle R_{N_2}^2\rangle \sim N_2^{2\nu}$$

$$\log\left(\frac{\langle R_{N_1}^2\rangle}{\langle R_{N_2}^2\rangle}\right) \sim 2\nu\log\left(\frac{N_1}{N_2}\right)$$

$$\varphi_{R^2} = \frac{\log\left(\frac{\langle R_{N_1}^2\rangle}{\langle R_{N_2}^2\rangle}\right)}{\log\left(\frac{N_1}{N_2}\right)} \tag{2.12}$$

For large $N \to$, the crossing point of curves φ_{R^2} is expected to predict structural phase transition point.

At low $J < J_\theta$, the system is equivalent to SAW without interaction. One should call to mind the classical homopolymer model which is represented by an interacting, or collapsing, self-avoiding walk

(iSAW). Below we briefly report known critical values for homopolymer which are important in our work as iSAW is a parental model of XY on SAWs.

2.2.1 SAW on a 2D square lattice

Focus on collapsing self-avoiding walks, or classical homopolymer model (see chapter 9 in Ref.[1]. At $J = 0$, spins become irrelevant and XY model on SAWs is equivalent to non-interacting SAWs. The exact value of critical exponent for non-interacting SAWs ($J = 0$)[20]

$$\nu = \frac{3}{4}. \tag{2.13}$$

At the theta-point, ν_θ is obtained via Coulomb-gas approximations [21]:

$$\nu_\theta = \frac{4}{7}. \tag{2.14}$$

For the globular regime ($J > J_\theta$) in 2D case:

$$\nu = \frac{1}{d} = \frac{1}{2}. \tag{2.15}$$

2.2.2 SAW on a 3D cubic lattice

For 3D case, Flory predicted value for non-interacting self-avoiding walk as follows [22]:

$$\nu = \frac{3}{2+d} = \frac{3}{5}. \tag{2.16}$$

The critical exponent ν was also estimated numerically [20]:

$$\nu = 0.5877 \pm 0.0006. \tag{2.17}$$

At the theta-point, the ν_θ is [1]

$$\nu = \frac{1}{2}. \tag{2.18}$$

For compact regime when $J > J_\theta$, the critical exponent ν has following value:

$$\nu = \frac{1}{d} = \frac{1}{3}. \tag{2.19}$$

3 Methods

3.1 Markov chain Monte Carlo methods

One common way to effectively simulate systems with a large number of degrees of freedom is to apply Monte-Carlo simulations [23].

We apply the Metropolis Monte Carlo method based on Markov chain. The main idea is to construct a Markov chain which has the given probability distribution (2.2) as its equilibrium distribution . In Markov chain Monte Carlo methods (often referred to as MCMC methods), the next sample is dependent on the last accepted one.

We use the Metropolis algorithm [24]. For generating an appropriate random set of states according to the given probability distribution (2.2), the conditions of ergodicity and detailed balance should be placed on the Markov chain. Ergodicity means that algorithm can generate any state u_{new} from any other state u_0 in a finite number of steps. In physics the detailed balance means that each elementary process is in equilibrium with its reverse process. Detailed balance condition can be written as follows:

$$p_{u_0} P(u_0 \to u_{new}) = p_{u_{new}} P(u_{new} \to u_0), \tag{3.1}$$

where $P(u_0 \to u_{new})$ is the transition probability from state u_0 to u_{new}. Here, $p_{u_0}, p_{u_{new}}$ are stationary Gibbs distribution probabilities: $p_{u_0} = e^{-H(u_0)}/Z$. Following a common way, we introduce the acceptance ratio $A(u_0 \to u_{new})$ and write:

$$P(u_0 \to u_{new}) = g(u_0 \to u_{new}) A(u_0 \to u_{new}),$$

where $g(u_0 \to u_{new})$ is the selection probability that algorithm will generate a state u_{new} from an initial state u_0.

3.1.1 Monte Carlo for self-avoiding walks

The self-avoiding walks model was studied before by several methods. The methods to generate states could be divided into two groups, referring to fixed-length ensembles and variable-length ensembles.

One of the trivial methods for sampling chains of fixed length slithering-snake, or BEE reptation, move [25]. The idea is to delete a node from one end of the walk and add a new node at the other end of conformation. We implement this update for XY model and discuss in Section 3.2.1.

One of the variable-length algorithms is the Beretti-Sokal method [26]. The algorithm has two types of elementary updates: positive move and negative move. The positive step is implemented by appending an edge to the endpoint of the conformation. The negative update is deleting the last edge. The algorithm is easy to implement and allows to study properties of self-avoiding ensembles and extract general properties, such as critical exponent ν from (2.11). However, these method is inefficient for studying region of structural phase transition in interacting self-avoiding walks [27] and the simplest heteropolymer [9]. Efficient degradation stems from the form partition function for grandcanonical assemble.

The other is well-know and widely used methods is growth algorithms. The review of growth algorithms is made thanks to Prelberg's material [28].

The most trivial way to generate SAWs is to use Simple sampling. The algorithm starts from the origin point and each step attempts draw one of the neighbouring sites chosen randomly using uniform distribution. If the site is occupied, the algorithm rejects walk and starts again from the beginning. This method is easy to implement and its samples are uniform and independent. But the method is inefficient due to a large number of rejections caused by collision.

One more sophisticated growth method is Rosenbluth Sampling. This method based on the steps when algorithm attempts to draw one of the unoccupied neighbouring sites chosen randomly and uniformly from the origin points and aims to generate the SAW of the chosen N. If there is none of non-visiting sites, the algorithm rejects entire walk and start again. The visiting only unoccupied neighbouring leads to increasing performance. However, the number of wasted attempts is still large. Grassberger introduced Pruned and Enriched Rosenbluth Method (PERM) with a vie to improve sampling [29]. Its modification is controlling the weights of SAWs copying (enrichment) states with large weights and occasional removing (pruning) conformations with low weights.

One of improved versions of PERM is flat histogram PERM (flatPERM) based on the fact that number of samples generated by PERM algorithm for each N is roughly constant. The method generates flat histogram algorithm in system size and allows to calculate the coefficients of the series expansion in terms of the dependent variables on J. This method was applied to simulate Ising model on SAWs [12]. FlatPERM is an efficient Monte Carlo method which allows to get functions of J and avoid analyzing of the separate points. However, the method gets slower for large N.

We choose to implement snake-like, or BEE reptation, move to generate structural states with the aim to simulate large N which would be quite difficult in practice using sophisticated FlatPERM. In order to improve sampling of SAWs, we also implement other update. In the Section 3.2, we discuss implement method applied to study XY model on SAWs.

3.2 MCMC of three updates

In this work, we construct the Markov Chain Monte Carlo method for fixed-length chain consisting of three types of updates. We refer to them as Snake-like step, Reconnection and Wolff Cluster update. In each iteration, the algorithm chooses the update according to set of probabilities. We define these probabilities as P_{local},$P_{reconnect}$ and P_{Wolff} respectively. The sum of probabilities is always equal to one: $P_{local} + P_{reconnect} + P_{Wolff} = 1$. This algorithm was described and used to study Ising model on SAWs [13].

3.2.1 Snake-like algorithm

This is classical method to generate SAWs which brings to mind snakes move [18]. The snake move is a bilocal reptation update. The algorithm removes a monomer from one end and adds a monomer to the other end as it is illustrated in Figure 3.1a. Spin angle value θ_{new} and the direction in conformation are randomly generated. The direction is chosen uniformly with the probability $\frac{1}{2d}$, where d is the dimensions of the lattice. The spin angle variable θ_{new} is generated uniformly $\theta_{new} \sim U(-\pi, \pi)$. The new generated state is simply accepted according to the Metropolis rule:

$$A(u_0 \to u_{new}) = \begin{cases} e^{-J(E_{u_{new}} - E_{u_0})}, & \text{if } E_{u_{new}} - E_{u_0} > 0; \\ 1, & \text{otherwise.} \end{cases} \tag{3.2}$$

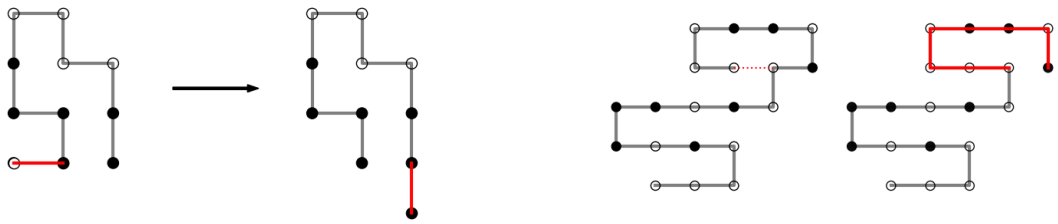

(a) Example of snake update.

(b) Example of reconnect update.

Figure 3.1: Examples for both algorithm moves: snake-like and reconnect. These updates allow to generate conformations.

The snake update is very convenient to implement and the time and the memory complexity $O(1)$. However, the autocorrelation time is quite long for magnetic variables and for structure $\eta \sim N^2$ and the system can be locked in the frozen states when both ends of the conformation are surrounded by $2d$ neighbors. To overcome the problem, we also use Reconnect update to accelerate conformations generation and Wolff-cluster algorithm to effectively explore spin configuration space.

3.2.2 Reconnect

Reconnect is a non-local update based on ideas of Worm algorithm for Ising model 3.1b [30]. In this system update, only connections of conformation are changed. The acceptance probability is always equal to one as the energy does not change.

The algorithm allows system to return from frozen stated. The reconnect algorithm also allows to effectively generate conformations. The time complexity $O(N)$.

3.2.3 Wolff cluster update

This is classical The Wolff algorithm for Monte Carlo simulation which we use to improve sampling of the spin configuration space [31].

The main idea of the update is to form the cluster C of spins and flip its spins. The update rules should obey the detailed balance condition. We follow the classical way of cluster update implementation for XY model discussed in Ref. [23].

To flip spin using chosen direction $\vec{n}$ means to change sign of vector $\vec{n}\vec{S}_i(\theta_i) = \vec{n}(\cos\theta_i \sin\theta_i)$ to the opposite, see Figure 3.2a.

1. Choose randomly the spin $\overrightarrow{S_{start}}$ from the chain using discrete uniform distribution.
2. Choose the direction on the unit circle $\overrightarrow{n}$ using uniform distribution $\theta_{new} = U(-\pi, \pi)$: $\overrightarrow{n} = [\cos(\theta_{new}), \sin(\theta_{new})]$.
3. Update the chosen monomer $\overrightarrow{S_{start}}$. To do it, we need to change sign of $\vec{n}\,\overrightarrow{S_{start}}$ to the opposite. This action is the subtraction the reflected $\vec{n}$ from $\overrightarrow{S_{start}}$. Therefore, the flip is implemented as following: $\overrightarrow{S_{start}} := \overrightarrow{S_{start}} - 2 \times (\overrightarrow{S_{start}}\,\vec{n}) \times \vec{n}$. We add this flipped spin to the cluster C and point it as flipped.
4. Take one spin $\overrightarrow{S_i}$ from the cluster to visit all its neighbors S_j, see Figure 3.2b. Add new spin to the cluster with the probabilities $P_{add}(\overrightarrow{S_i}, \overrightarrow{S_j}) = 1 - \exp\left(2J(\overrightarrow{S_i}\ \overrightarrow{n})(\overrightarrow{S_j}\ \overrightarrow{n})\right)$, where $\overrightarrow{S_i}\ \overrightarrow{n}$ is a dot product.

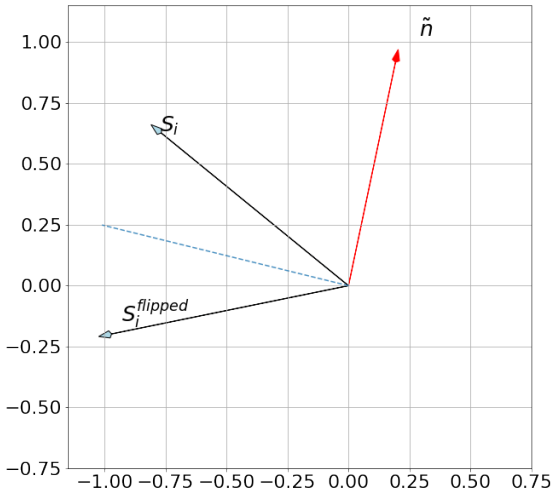

(a) Example of spin flip. The solid red arrow is randomly chosen unit vector $\vec{n}$. The dashed blue line is perpendicular plane

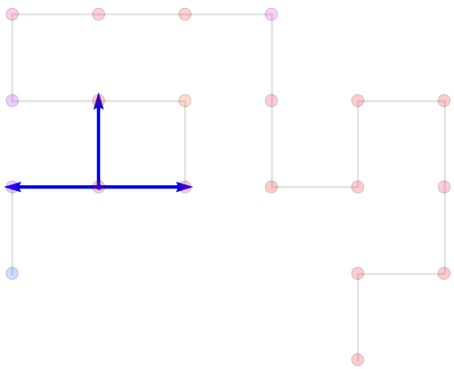

(b) Example of cluster grow from the starting point. Blue arrows shows directions to attempt to add new spins to cluster. The color of nodes represents spins values.

Figure 3.2: Cluster Update for XY on SAWs.

If the spin $\overrightarrow{S_j}$ was added to cluster and has not been flipped, make update: $\overrightarrow{S_j} := \overrightarrow{S_j} - 2 \times (\overrightarrow{S_j}\,\vec{n}) \times \vec{n}$. Point the spins as flipped.

After visiting all neighbors, remove $\overrightarrow{S_i}$ from the cluster.

5. Repeat the previous step until cluster is empty.

The algorithm effectively sample spin configurations and keep the conformation fixed. The time complexity $O(N)$.

4 Results

We implement Monte-Carlo algorithm 3.2 in C++ and push to the open GitHub repository [32]. Numerical simulations were done using the computational resources of HPC facilities at HSE University [33].

4.1 XY model on SAWs, 2D

To perform MC simulations for short chains from $N = 100$ to $N = 1000$, we run at least 2.1×10^9 MC steps using two types of updates: snake-like and reconnect. We choose following update probabilities: $P_{local} = 0.8$, $P_{reconnect} = 0.2$.

For longer chains $N > 1000$ we additionally use cluster update. We simulate chains up to $N = 4900$. For $N = 4900$, we run at least 8×10^{10} MC steps. Here we use these values for update probabilities: $P_{local} = 0.8$, $P_{reconnect} = 0.199$, $P_{Wolff} = 0.001$. Despite both Reconnect and Cluster updates have complexity $O(N)$, we choose small P_{Wolff} due to slow iterations cause by using queue for creating cluster of spins. At average, the Reconnect is much faster and leads to get faster convergence of geometry properties, for example, mean radius.

4.1.1 Tests for validation simulations

To test our Monte-Carlo (M) simulation, we compare results obtained using MC and Sampling + Exact Enumeration (EE). The exact numeration is the generation of all self-avoiding walks of the particular low value N using recursion technique. As the space of spin configuration is continuous, we simply sample a number of vectors which components come from the uniform distribution $U(-\pi, \pi)$. For each generated SAW-conformation we generate the set of spin configurations. This allows to obtain mean values and sum generated sets to the partition function. This method is only approximation, but it helps to make approximate checks.

We calculate Mean Radius (2.10), mean energy (2.1) and second moment of magnetization (2.4) for short chains ($N = 5, N = 8$). The generation of spin configuration and applied it to the whole set of SAWs is resource-consuming procedure. Therefore, we sample spin configurations only 600 times (so, 600 sequences of spins applied to each conformation) and repeat this 10 times. Figure 4.1 shows obtained results. For $J = 0$, the second moment of magnetization are close to exact values (2.8) and the mean energy starts at $\langle e \rangle = 0$. Therefore, teh MC data in a good accordance with the expected values from Section 2.1.1.

The other way to validate implemented algorithm is to vary set of probabilities for updates which we denote as $(p_1, p_2, p_3) = (P_{local}, P_{reconnect}, P_{Wolff}$. The most important region for checking is critical region where physical quantities are dynamic. For non-interacting regime, the program could give correct values predicted analytically, but it does not help to avoid bugs in energy-dependent steps in iterations, such as calculating acceptance probability. For large J in should-be-compact-maybe-ordered phase, the physical properties are also quite stable and bugs are less obvious. It is a tricky moment that we need to have a correct implementation to find the critical region, but we need to know the critical interval to validate

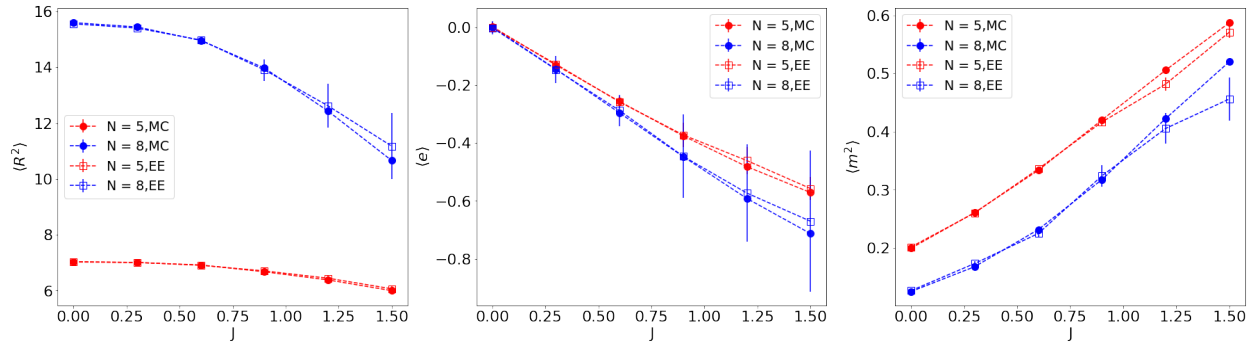

Figure 4.1: Mean Radius (2.10), mean energy (2.1) and second moment of magnetization (2.4).

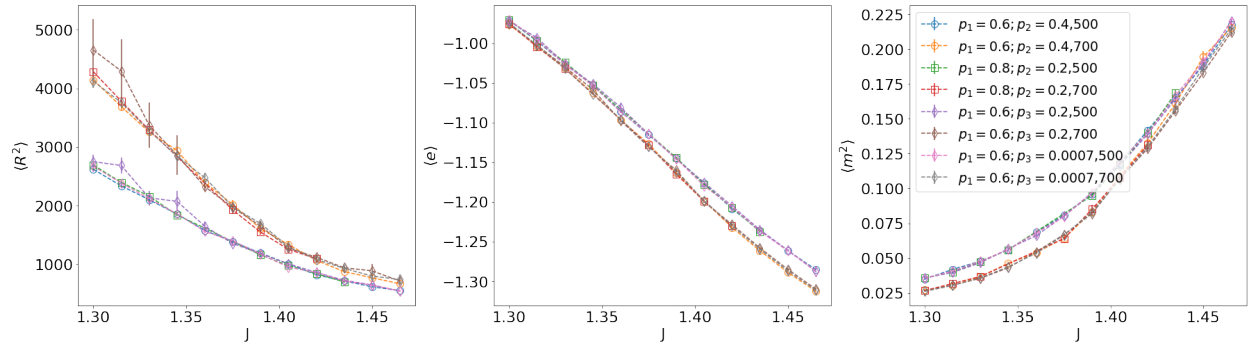

Figure 4.2: Mean Radius (2.10), mean energy (2.1) and second moment of magnetization (2.4) as functions of J on the critical region for two chains lengths $N = 500$ and $N = 700$. $(p_1 + p_2 + p_3 = 1$

programmed code and be sure that it is correct implementation. However, we can overcome it over iterations and narrowing critical region running short simulations for short chains.

To make final check of the written code for simulations, we run program for two chains lengths $N = 500$ and $N = 700$ at the narrowed region where the critical behavior is expected from previous short run. We vary J and perform simulations using four sets of (p_1, p_2, p_3). In two stets we do not use Cluster update to check its implementation separately. Figure 4.2 illustrates results of validation for three properties, mean Radius (2.10), mean energy (2.1), second moment of magnetization (2.4) as a functions of coupling constant J. For both lengths, the curves for each function overlap within combined errorbars.

4.1.2 Thermodynamic properties

First, we measure the mean square magnetization (2.4) and the mean energy (2.1) for short chains (up to $N = 1000$) in the large range of the interaction energy J and for long chains (up to $N = 4900$) in the narrow range where the system are expected to undergo the phase transition.

Figure 4.3 (left column) shows computational results for the mean energy (2.1) as a function of J. At the top plot for short chains, the mean energy starts at $\langle e \rangle = 0$ as expected for unfolded disordered SAWs.

Figure 4.3 (right column) illustrates obtained numerical results for the second moment of magnetization (2.4). At $J = 0$, results are consisted with the exact solution (2.8) and $\langle m^2 \rangle \to 0$ as $N \to \infty$. As J increases, the square of magnetization grows up. One can expect an ordering behavior for large J.

4.1.3 Structural properties

We start our studying structural properties of the model with visual inspection of the scaling function for mean radius (2.12). We calculate scaling ratios for different pairs of chain lengths N_1, N_2. In the model of

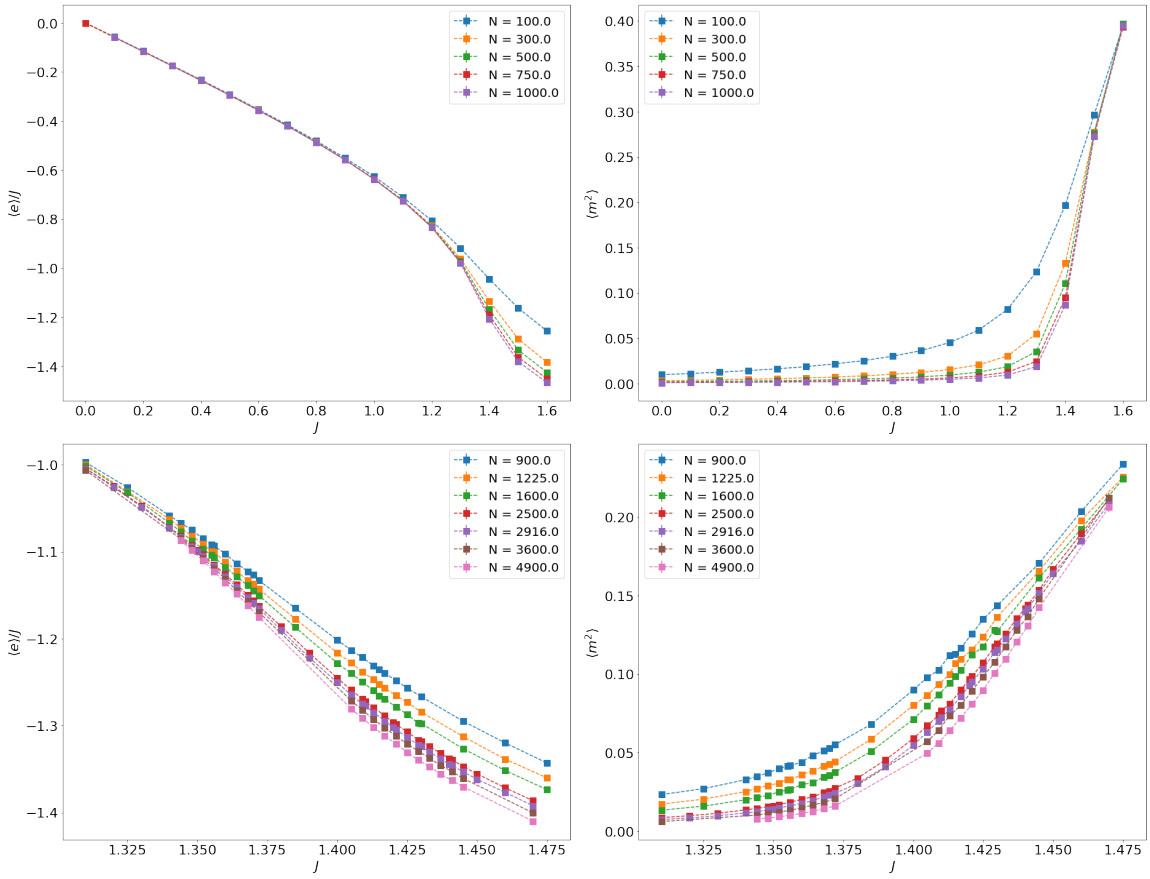

Figure 4.3: $h = 0$. Mean energy (2.1) and second moment of magnetization (2.4). Symbols are MC data with errors with dashed line as a guide to the eye.

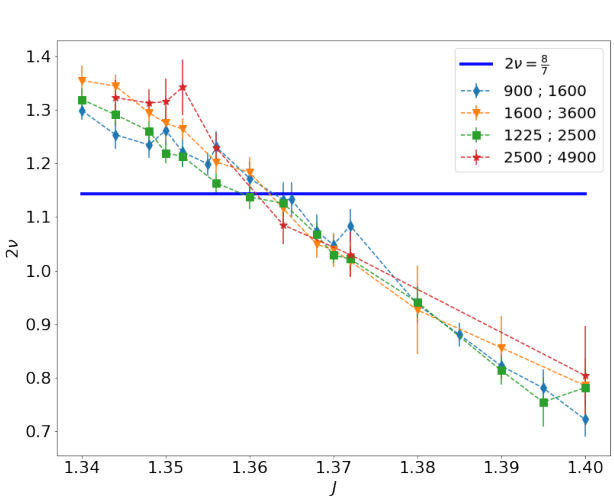

(a) Scaling function (2.12) as a function of J. The errorbars are computed via Gaussian sampling.

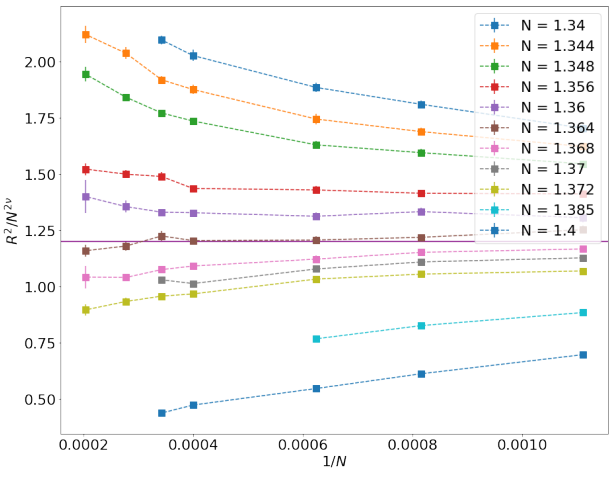

(b) Scaled Mean-squared end-to-end distance using $\nu_\theta = 4/7$ as a function of $1/N$ from $N = 900$ to $N = 4900$.

Figure 4.4: Visual inspection of scaling of mean radius. The purple horizontal line corresponds to structural phase transition.

classical interacting SAWs without spins, the curves cross at the structural phase transition point and at the critical value of exponent ν. In this step, our obtained computational data for XY on SAWs 4.4a do not contradict the assumption that value ν is inherited from the iSAW model. However, we cannot make estimation of crossing point due to large errorbars.

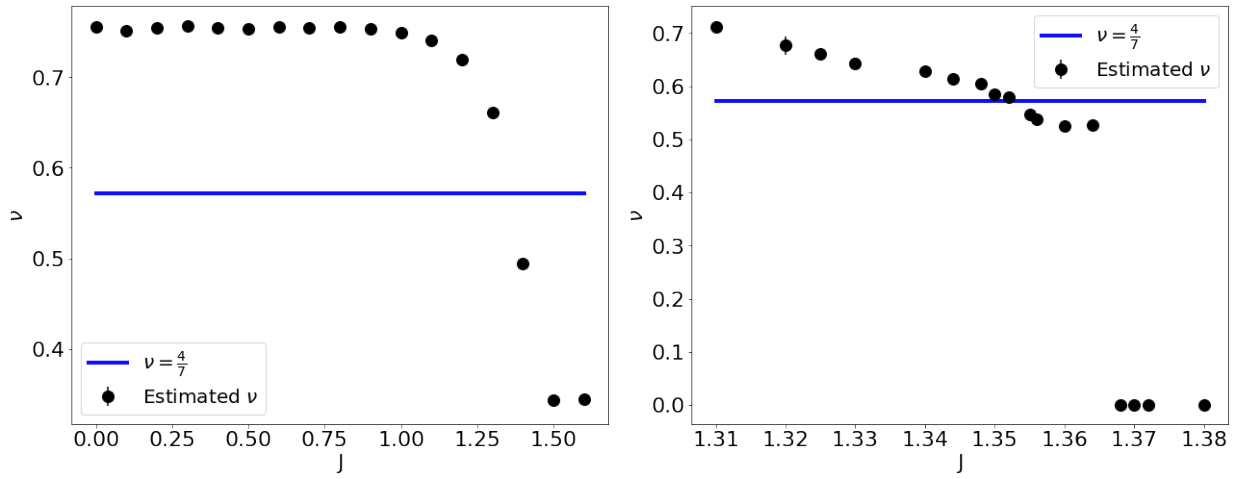

(a) From $N = 100$ to $N = 1000$.

(b) From $N = 1225$ to $N = 4900$.

Figure 4.5: Estimates with errorbars of critical exponent ν via (4.1) .

Figure 4.4b shows the scaled mean-squared end-to-end distance by $\nu = 4/7$ as a function of $1/N$ for different J. The horizontal line is placed at the estimation from Section 4.1.4. This line corresponds to the structural phase transition point.

Next, we estimate critical exponent ν (2.11) from the asymptotic power law for the mean square end-to-end distance of SAWs. We use following ansatz [26]:

$$\log(R_N^2 + k_1) = 2\nu \log(N + k_2) + b. \tag{4.1}$$

Here $k_1 = k_2 = 1$ are phenomenological parameters.

For the start, we perform curve-fitting for short chains on the large range of values J. Figure 4.5 illustrates obtained results of exponent estimation. In $J = 0$, the critical exponent ν equals $\nu = \frac{3}{4}$ which is consisted with the value of non-interacting SAWs (2.13). The value $\nu = \frac{4}{7}$, which is the exact value for interacting SAWs (2.14), appears at the region $1.25 < J < 1.4$ (Figure 4.5, left part). Despite effects of finite size, we can create the idea that structural phase transition happens at the $J \in [1.32; 1.37]$ (Figure 4.5, right part).

We thus use that XY model on SAWs also has value $\nu = 4/7$ (2.14) at the point of structural phase transition. We use this value to obtain collapsing plots in Figure 4.6 in following subsection 4.1.4.

4.1.4 Transition

To focus on studying phase transition, we calculate two characteristics. The first one is the mean square end-to-end distance scaled using the factor $\nu = \frac{4}{7}$ in (2.11). The second one is Binder cumulant of magnetization (2.5). Figure 4.6 presents obtained calculations.

Magnetic phase transition

We compute Binder cumulamts (2.5) with the aim of determining order of magnetic transition.

The Binder cumulants (top Figure 4.6b) has lower limiting value $U_4 = \frac{1}{3}$ as $J \to 0$ which is in a good agreement with analytically obtained value in Section 2.1.1. For large interaction energy constant J, the system signs ordering behavior, as expected, $U_4 = \frac{2}{3}$.

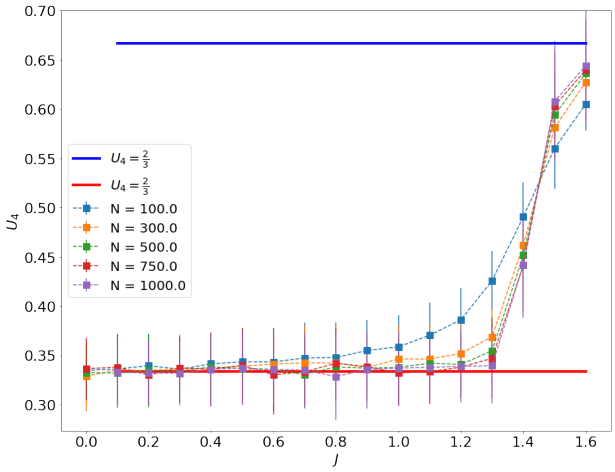

(a) Binder cumulant on the wide range of J with both lower and upper limits.

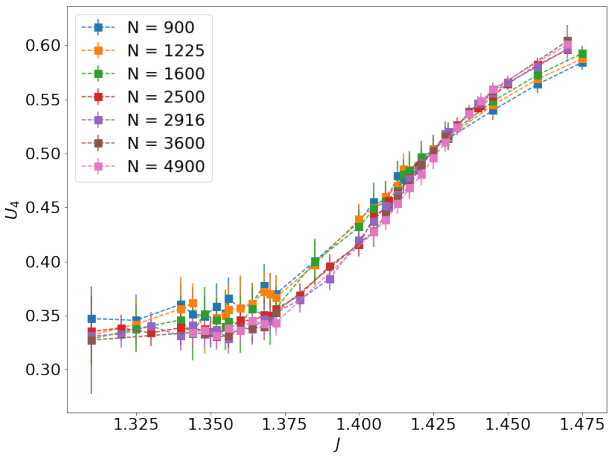

(b) Binder cumulant for long chains on the critical region

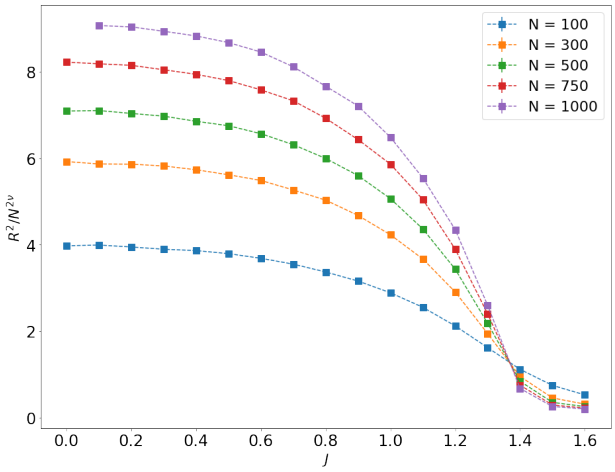

(c) Scaled mean radius from simulations short chains

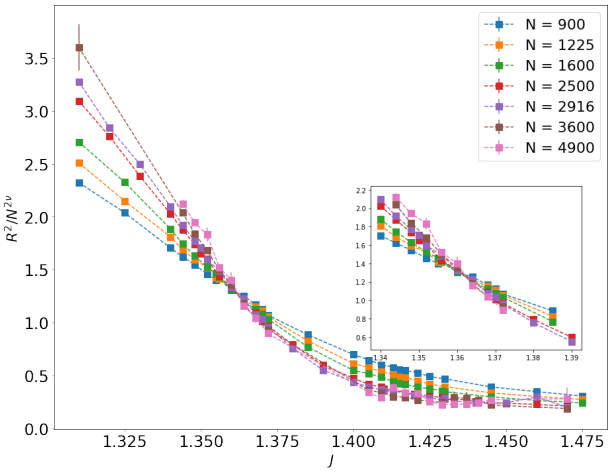

(d) Scaled mean radius with zoom-in at the critical interval

Figure 4.6: Binder cumulants (2.5) and mean radius (2.10) scaled by $\nu = \frac{4}{7}$.

Figure 4.6b shows that Binder parameter curves does not diverge. Therefore, our computational results do not detect the first-order transition. Figure 4.7a illustrates cumulants in the narrow region where curves cross. Binder parameter are represented as a function of $1/N$ in figure Figure 4.7b varying J. The horizontal line should correspond the critical point. However, due to large errobars and finite-size corrections, we cannot determine $J_c r$ place according to this plot.

To estimate critical values for cumulants U_4 and phase transition point J_{cr}, we perform paired linear intersections. The procedure to analyze Monte-Carlo data is following:

1. Choose the pair of two different N values for length of the chain. Choose the range of values for interaction energy J. This segment should be as short as possible and include the point of intersection of the two curves.

2. We need to obtain the errors to estimated Binder cumulant. To that end, we use Gaussian sampling.

For each point from the set generate $n_{samples}$ values using Normal distribution with mean and standard error of $\langle m^2 \rangle$ and $\langle m^4 \rangle$ as parameters: $M2_{J,N} \sim N(\langle m^2 \rangle, \sigma(\langle m^2 \rangle))$, $M4_{J,N} \sim N(\langle m^4 \rangle, \sigma(\langle m^4 \rangle))$. We generate for each value J 1000 samples. For each pair of sampled m_2, m_4 we calculate the Binder cumulant (2.5).

3. Using generated set, for each pair J and N make estimation for mean and standard deviation $\langle U_4 \rangle$.

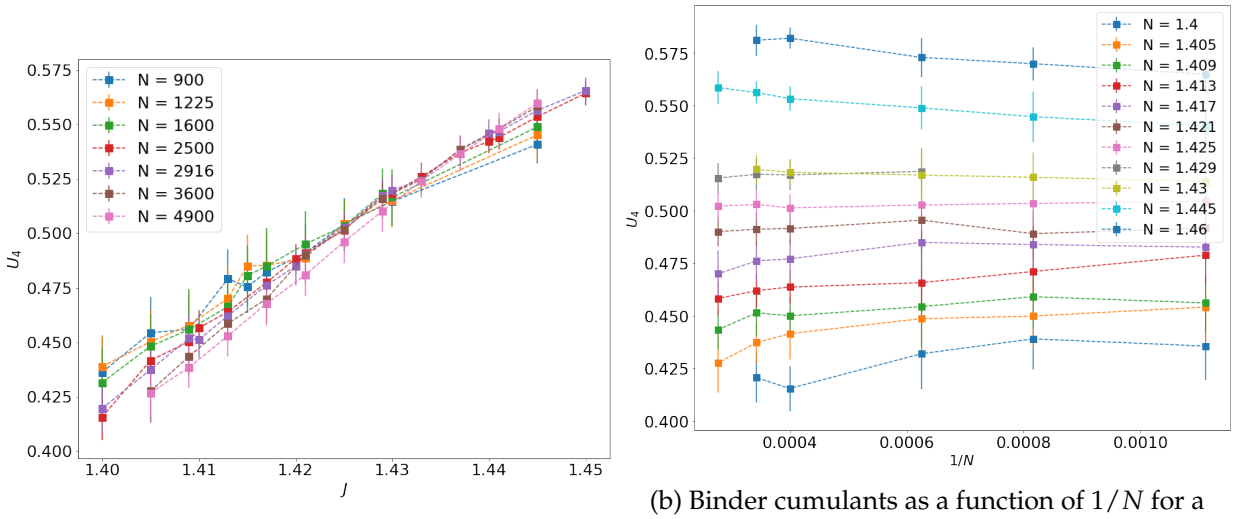

(a) Zoom-in of Figure 4.6b.

(b) Binder cumulants as a function of $1/N$ for a range of J.

Figure 4.7: Binder cumulants at the critical region.

4. Now, we have two curves of calculated U_4 with errorbars for two values of N. Apply weighted least squares regression to find crossing point. Save the obtained estimation for $\hat{J}$.

5. Repeat steps 2-5 n_{lines} times. We repeat it $n_{lines} = 1000$ times.

6. At the end, we have n_{lines} of estimated $\hat{J}$ where two curves cross.

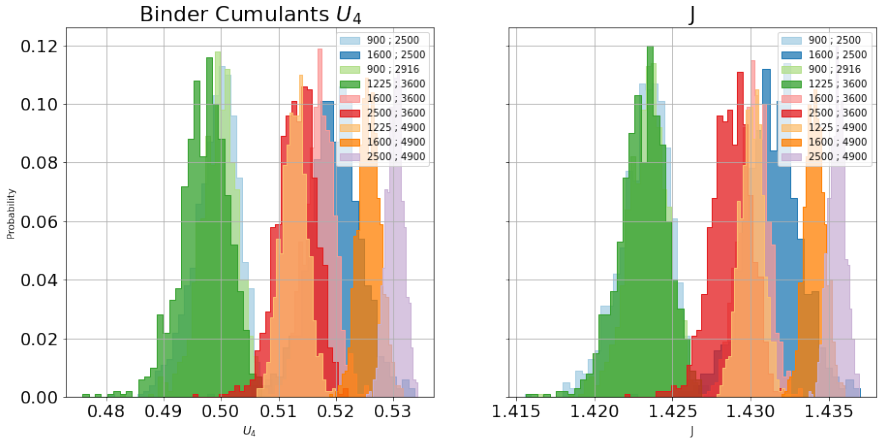

Figure 4.8: $h = 0$. Histograms of estimated U_4 and J_{cr} from paired regressions.

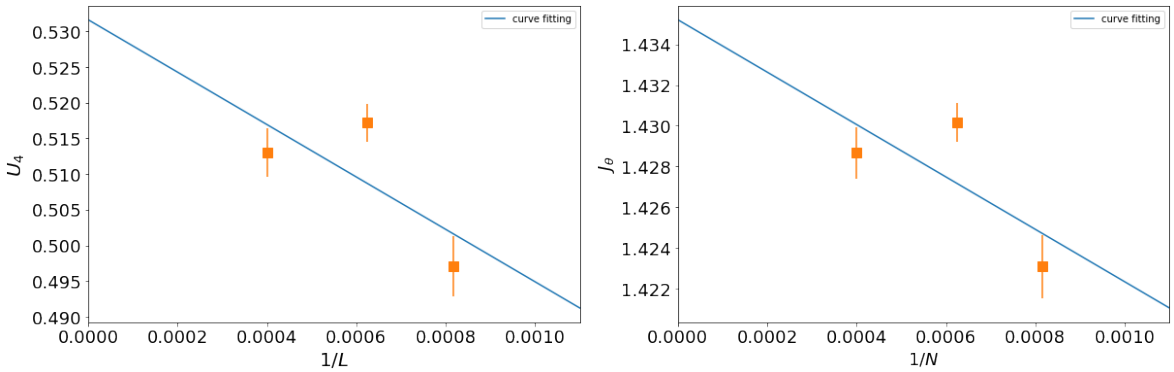

Figure 4.9: Histograms of estimated U_4 and J_{cr} from paired regressions with $N = 3600$.

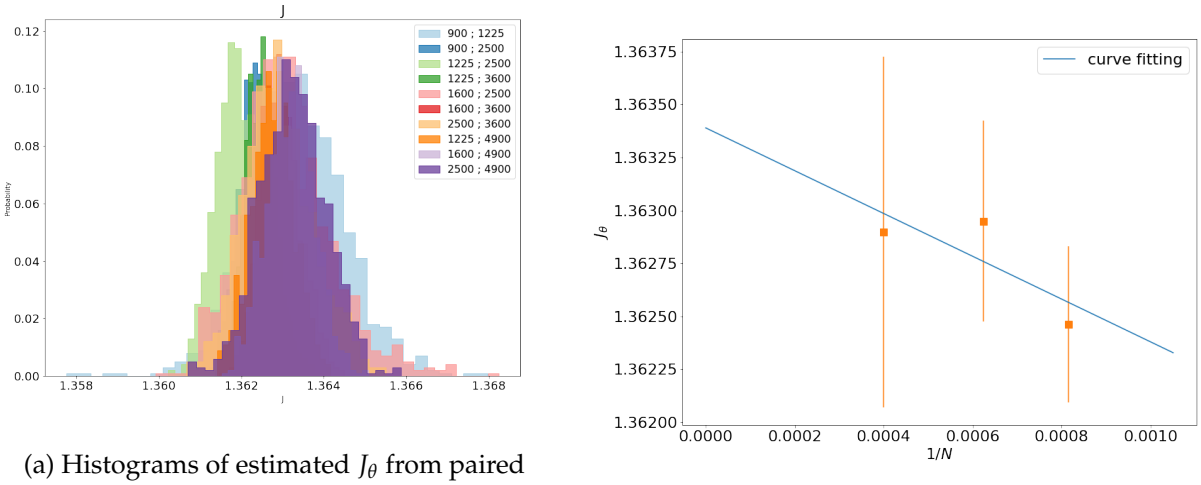

(a) Histograms of estimated J_θ from paired regressions.

(b) Crossing points using pairs with $N = 3600$.

Figure 4.10: Estimate for J_θ using pairs for $N = 3600$.

Histograms for pairs from Figure 4.8 shows us how the size of systems affect the estimations $\hat{J}$. One way to choose the estimation for phase transition point $\hat{J}$ in thermodynamic limit is to focus on pairs for long chains with not too large errorbars. We choose $N = 3600$.

Consider the set of results for $N = 3600$. We have calculations for four pairs $[N_i, 3600]$ which presented in Figure 4.8. We construct the dependence of estimates $\hat{J}_\theta$ on $1/N_i$. Using this measurements, we perform curve-fitting using weighted least squares regression. The fitting results are plotted in Figure 4.9. Estimation of critical point is the point of the limit $1/N_i \to 0$. The errorbars are calculated using module *linregress* from SciPy. We obtain the following results:

$$J_{cr}^{3600} \approx 1.43519999570142 \pm 0.0079203 \tag{4.2}$$

The estimation of critical value of cumulant at the magnetic transition is following: $U_4 \approx 0.55(5)$. This value is far from the Binder cumulant value for classical Ising model on the square lattice with periodic boundary condition and for Ising model on SAWs in 2D [13].

Figure 4.9 shows that the Binder cumulant of crossing points for $N = 3600$ is increasing with using larger second chain size. The same dependence on system size was found in studying XY model on square lattice at KT transition [34].

Estimation of $\hat{J}_\theta$

In the bottom of Figure 4.6 we can see that scaled curves of mean radius for range of N values cross approximately at the same point. To estimate the point of structural phase transition, we repeat the procedure with histograms for paired linear crossings described in Section 4.1.4, except for step 2.

Repeating the linear fitting results Figure 4.10b, we obtained following estimated value from the zero point:

$$J_\theta^{3600} \approx 1.3633900514712 \pm 0.00050. \tag{4.3}$$

Our computational results shows that magnetic transition (4.2) and structural transition (4.3) appears at the different points. The intervals within errobars do not overlap. Therefore, we cannot conclude that magnetic phase transition and structural transition happens at the same point, in contrast to Ising model on

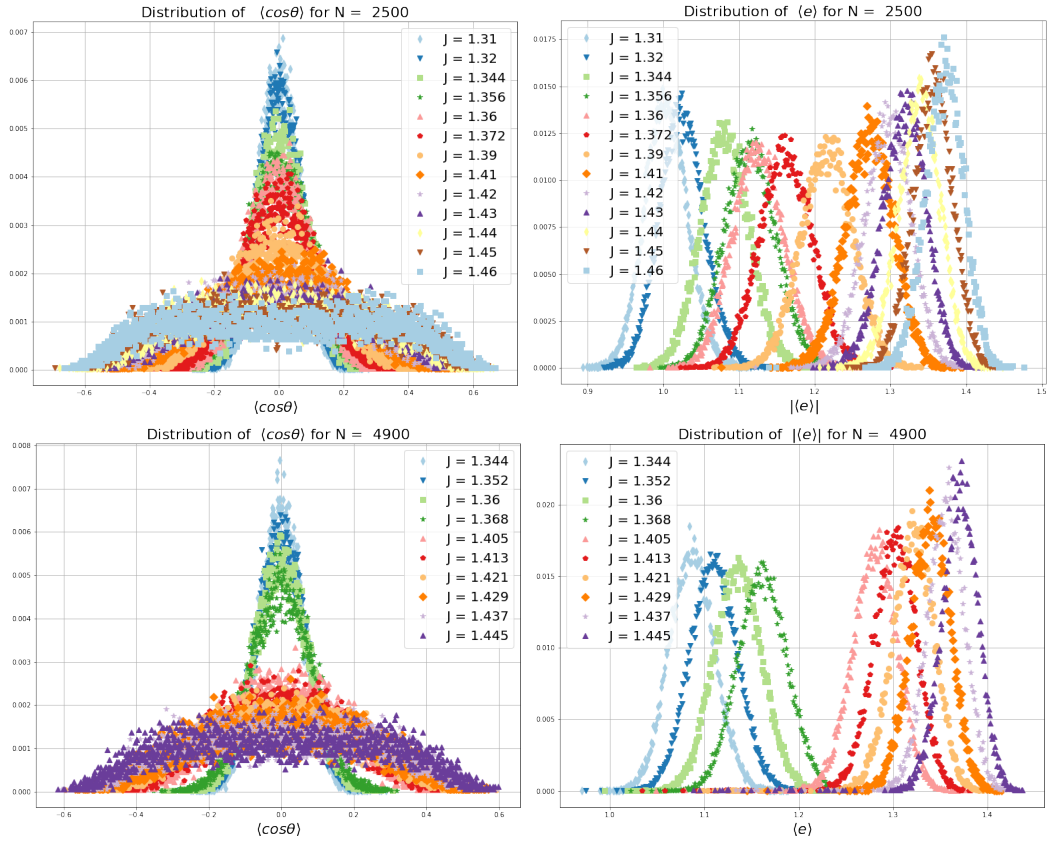

Figure 4.11: Distributions for chains $N = 2500$ and $N = 4900$ for various J.

SAWs. Our MC the data is inconclusive, whether the transitions occur simultaneously or at distinct values of the coupling constant J. More work is needed to conclusively rule out one of possibilities.

4.1.5 Distribution of $\langle cos\theta \rangle$ and $\langle e \rangle$

To study the phase transition order, we look to distributions of energy and magnetization.

Figure 4.11 shows shapes of energy distribution across the structural transition (4.3) and magnetic transition (4.2). The curves of distributions is Gaussian-like and do not sign any bimodal shapes.

Additionally to energy, we consider mean $\cos\theta$ which represents a component of mean magnetization vector (2.3). For points $J < J_{cr}$, curves of $\cos\theta$ distribution is similar to normal curve. Over the critical region, the shapes of distributions are far from Normal-like curves. Here we cannot conclude whether there is some signs of phase coexistence or not.

4.1.6 Summary for 2D case

We study XY model on self-avoiding walks on the square lattice (2D case) using Monte-Carlo simulations. In this work, we consider regime when both conformations and spins are dynamic. Obtained numerical result do not show signs of first-order transition. We cannot conclude that magnetic phase transition (4.2) and structural transition (4.3) happens at the same region, in comparison to Ising model on SAWs. Our MC the data is inconclusive, whether the transitions occur simultaneously or at distinct values of the coupling constant J. More work is needed to conclusively rule out one of possibilities.

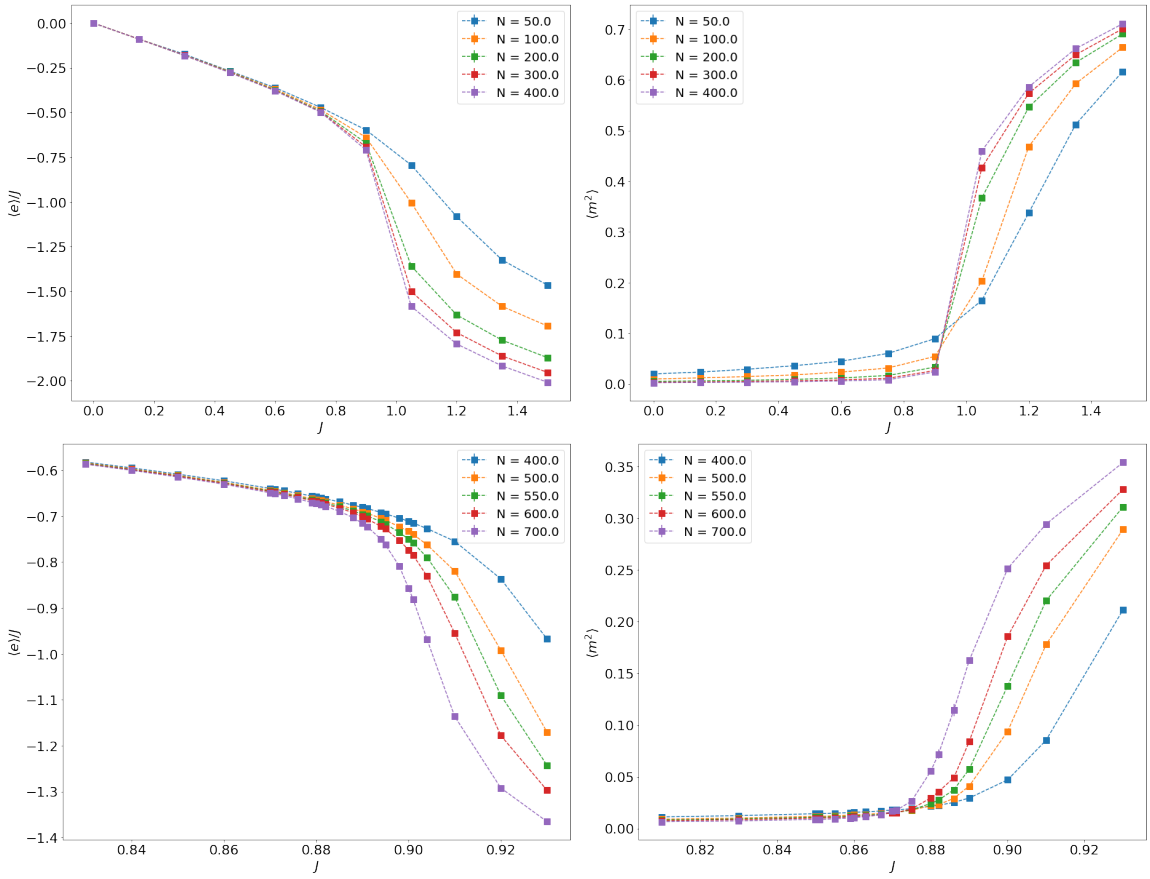

Figure 4.12: $h = 0$. Mean energy (2.1) and second moment of magnetization (2.4).

4.2 XY model on SAWs, 3D

Here, we study XY-model on SAWs on the cubic lattice. The sequence of our actions is similar to investigation of 2D case.

In this section, we consider short chains up to $N = 700$ which is much shorter than we study for 2D case. The reason of it is the lattice implementation which requires to keep $2dN^3 = 6N^3$ nodes in the memory.

We make short MCMC simulations for short chains from $N = 50$ to $N = 300$ to narrow the region of critical behavior. MC steps. We use following values for update probabilities: $P_{local} = 0.6$, $P_{reconnect} = 0.499$, $P_{Wolff} = 0.001$. For $N = 300$, we run at least 1.6×10^9 algorithm iterations.

For longer chains from $N = 400$ to $N = 700$ we use these values for update probabilities in the algorithm: $P_{local} = 0.5$, $P_{reconnect} = 0.4$, $P_{Wolff} = 0.1$. We run at least 8×10^{10} MC steps for $N = 700$.

In all runs, we skip first $400 \times N^2$ MC iterations as the system should achieve equilibrium. We save each 1000th sample to compute properties.

4.2.1 Thermodynamic properties

First, we measure the mean square magnetization (2.4) and the mean energy (2.1) to study the system.

The squared magnetization (right column in Figure 4.12) grows as the interaction energy J increases. This behavior is similar to 2D case.

The mean energy (left column in Figure 4.12) rapidly decreases for low-temperature regime which could be a sign of compact ordered phase.

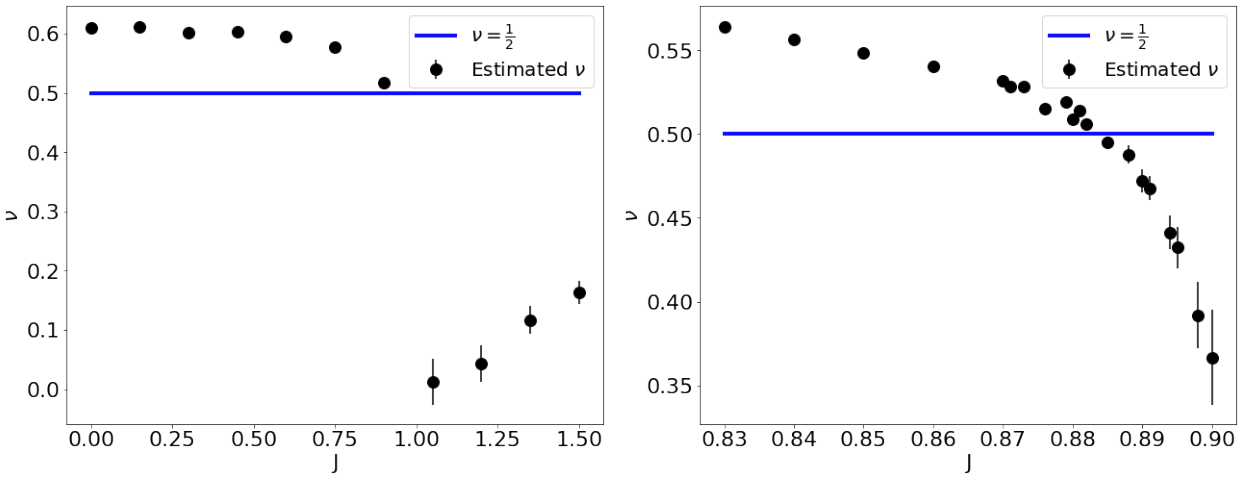

(a) From $N = 50$ to $N = 400$.

(b) From $N = 400$ to $N = 700$.

Figure 4.13: $h = 0$. Estimates with errorbars of critical exponent ν .

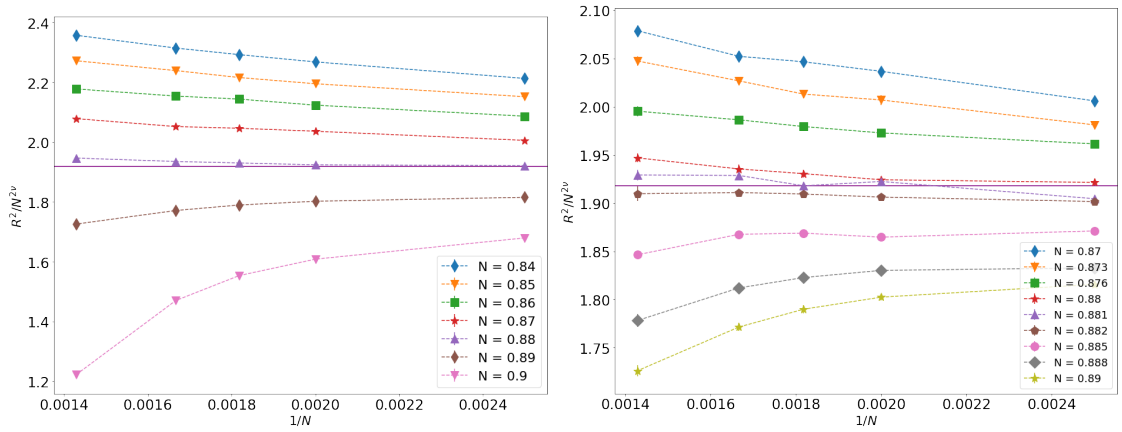

Figure 4.14: Scaled Mean-squared end-to-end distance using $\nu_\theta = 1/2$ as a function of $1/N$ from $N = 400$ to $N = 700$. The solid purple horizontal line corresponds to structural phase transition and placed at the estimation from Section 4.2.3.

From curves of both properties mean squared magnetization and mean energy, we can expect that the critical point is in the interval $J_\theta \in [0.84; 0.92]$.

4.2.2 Structural properties

Here we use the procedure from Section 4.1.3 to test the hypothesis that the critical exponent ν takes the proposed critical value (2.18) at the approximated critical region $J_\theta \in [0.84; 0.92]$.

Figure 4.13 illustrates the obtained results for ν estimations. In the non-interacting regime $J = 0$, we get $\nu \approx 0.6(1)$ for the short chains from $N = 50$ to $N = 400$. This result is close to Flory prediction (2.16). We also see that the possible critical value (2.18) appears approximately at the region $J_\theta \in [0.87; 0.89]$.

Figure 4.14 shows the scaled mean-squared end-to-end distance by $\nu = 1/2$ as a function of the chain length $1/N$for a range of J. The horizontal line is expected to represent the point of structural phase transition and corresponds to the critical exponent ν_θ. As the left part of the plot matches longer chains, we assume that the scaled curve of the mean radius at θ-point should be horizontal more at the left part. We place the horizontal line at the estimated value where scaled curves cross using histogram procedure. The horizontal line is limited by red star-marked curve ($J = 0.88$) and pink circle-marked curve ($J = 0.885$).

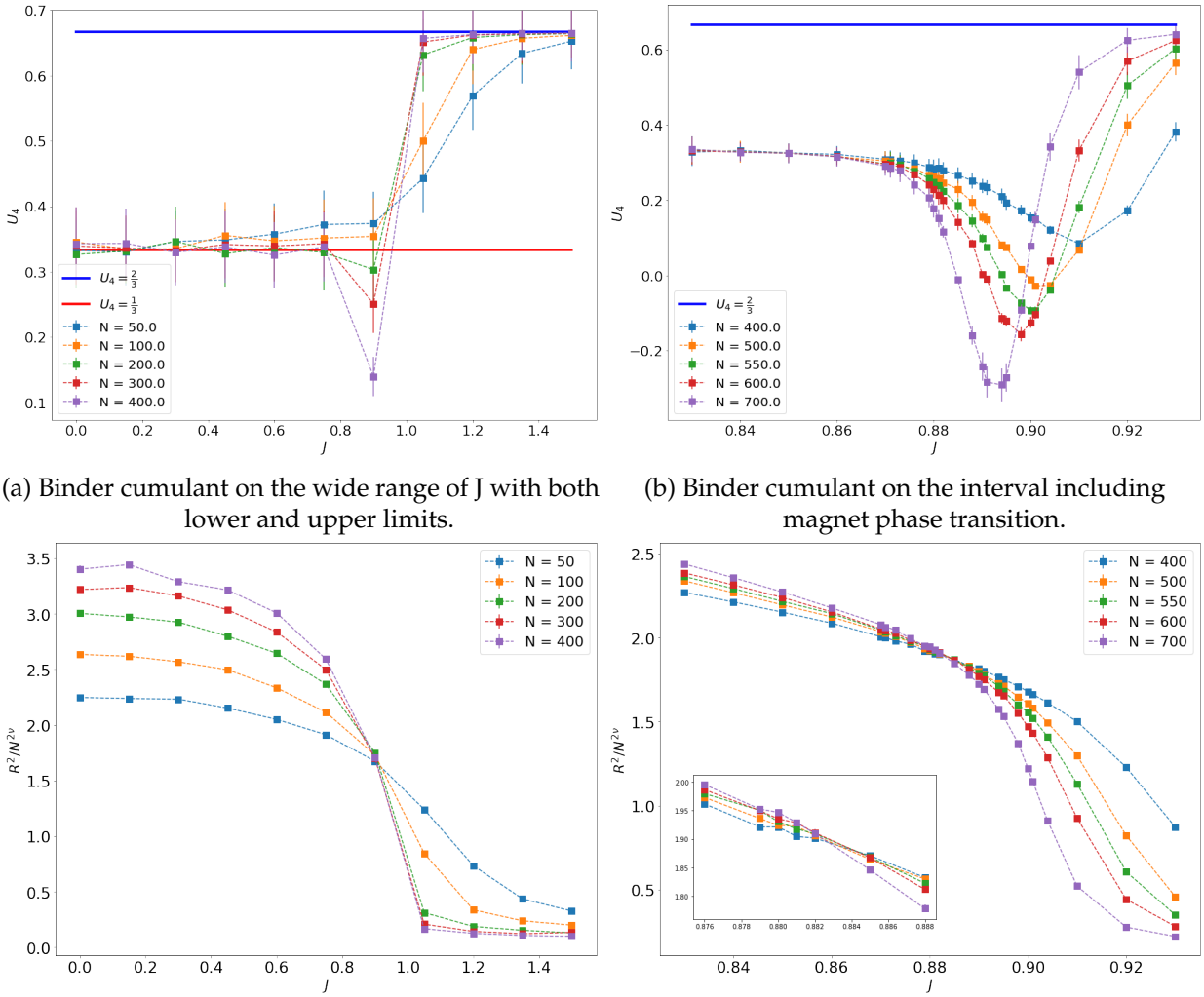

(a) Binder cumulant on the wide range of J with both lower and upper limits.

(b) Binder cumulant on the interval including magnet phase transition.

(c) Scaled mean radius for short chains on the large range of J.

(d) Scaled mean radius for long chains on the region with structural phase transition.

Figure 4.15: $h = 0$. Binder cumulants (2.5) and mean radius (2.10). The mean radius is scaled by $\nu = \frac{1}{2}$.

Therefore, according our calculations for chains up to $N = 700$, the system undergoes the structural phase $J \in [0.88; 0.885]$ with the critical exponent $\nu_\theta = \frac{1}{2}$. However, this visual inspection is not very reliable due to finite size effect.

For further study, we note the critical exponent value $\nu_\theta = \frac{1}{2}$ and use it in the following section to scale mean radius.

4.2.3 Transition

To investigate the critical behavior at the phase transition, we again calculate the Binder cumulants values (2.5) and scaled mean end-to-end distance (2.10). As predicted in Section 2.1.1, the Binder parameters (top Figure 4.15) has lower limiting value $U_4 = \frac{1}{3}$ as $J \to 0$. For large values of coupling constant J, the system gets the ordering phase, for which $U_4 = \frac{2}{3}$.

Cumulant curves diverges at the critical region. This is sign of the first-order phase transition [35]. The similar results for diverged cumulants were obtained for Ising model on SAWs for 3D case [12].

We check the distributions of thermodynamic characteristics in subsection 4.2.4 to check whether energy distribution is bimodal and magnetic distribution show signs of phase coexistence.

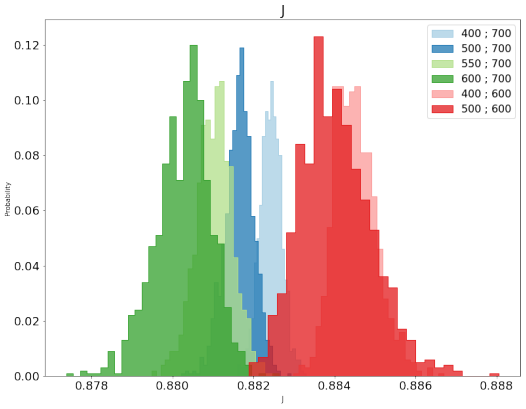

(a) Histograms of estimated J_θ from paired regressions.

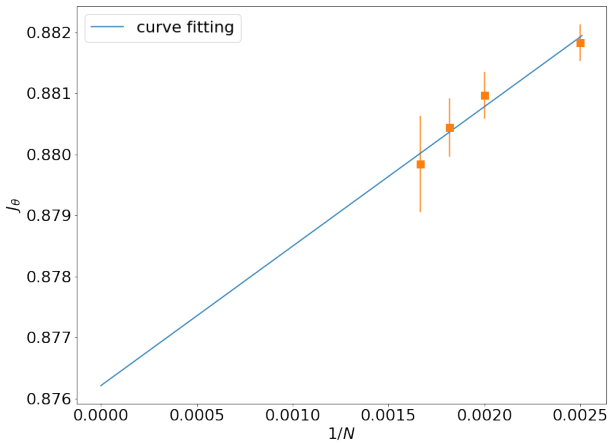

(b) Pairs with $N = 700$.

Figure 4.16: $h = 0$. Estimate for J_θ

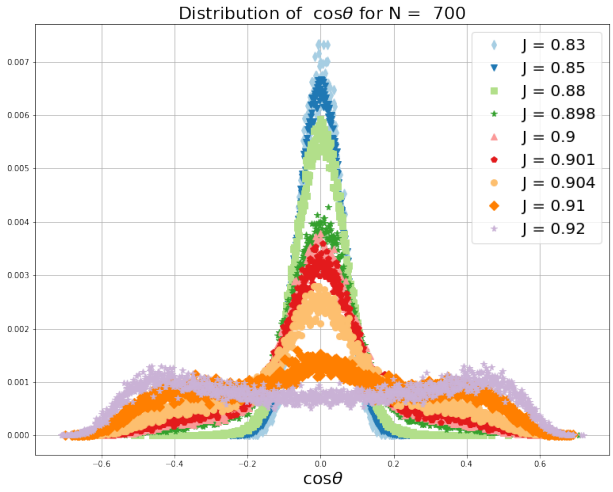

(a) The mean component $\cos\theta$ of magnetization vector.

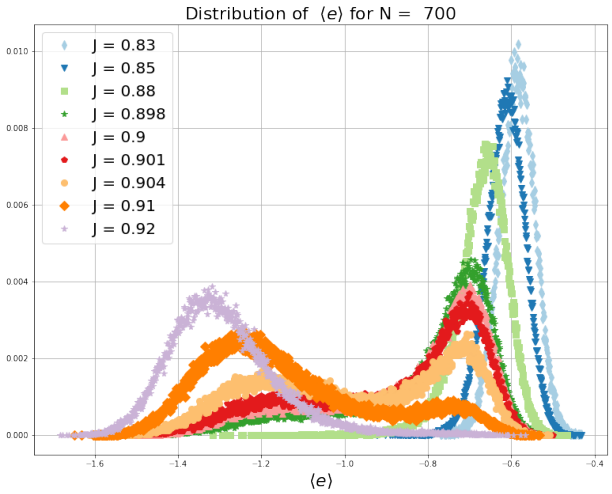

(b) The mean energy.

Figure 4.17: Distributions for chain $N = 700$ for various J.

Estimation of $\hat{J}_\theta$

We can estimate the critical value of the interaction energy J repeating the procedure described in the 4.1.4. Figure 4.16a shows us histograms for paired crosses.

The fitting results are plotted in Figure 4.16b. Estimation of critical point is the point of the limit $1/N_i \to 0$. We obtain the following value:

$$J_\theta^{700} \approx 0.876(5). \tag{4.4}$$

4.2.4 Distribution of $\langle cos\theta \rangle$ and $\langle e \rangle$

In the subsection 4.2.3 we concluded that XY model on SAWs has first-order phase transition according to the divergence of the Binder cumulants. Now we look at the distributions of the energy and magnetization to study it further.

Figure 4.17b illustrates that energy distribution has bimodal shape approximately at $J \approx 0.904$. However, this region of bimodal curve is quite far (≈ 0.03) from the estimation for point of the structural transition (4.4) and the divergence region of minimum Binder cumulant (see Figure 4.15a). This could be caused by finite size effect as chains up to $N = 700$ are not too long.

We consider mean $\cos\theta$ which is a component of mean magnetization vector (2.3). For points $J < J_{cr}$ before magnetic transition transition, curves of $\cos\theta$ distribution is similar to normal curve which is expected as this case corresponds to the sampling from uniform distribution $U \sim [-1;1]$ and convergence to the Gaussian.Over the critical region, the shapes of distributions are far from Normal-like curves.

4.2.5 Summary for 3D case

In this section, we present our computational results for XY model on cubic lattice. We simulated chains up to $N = 700$ to study system at the transition region. Our computational data indicates that XY model on SAWs in 3D has first-order magnetic transition from disordered phase to ordered state. The polymer system undergoes structural transition from denatured state to compact one at $J_\theta^{700} \approx 0.876(5)$.

5 Conclusion

In this project, we study XY model on self-avoiding walks on both square and cubic lattices. We consider regime when both conformations and spins are dynamic.

In order to study critical behavior of the model, we use Markov Chain Monte-Carlo method. We implemented the algorithm consisting of three types of updates: BEE-reptation move, Reconnection and Wolff cluster. We wrote our program in C++ and used HPC cluster in HSE university.

In study of 2D case, we made simulations for chains up to $N = 4900$. Our numerical result do not show signs of first-order transition. We cannot conclude that magnetic phase transition (4.2) and structural transition (4.3) happens simultaneously. Our MC the data is inconclusive, whether the transitions occur simultaneously or at distinct values of the coupling constant J. More work is needed to conclusively rule out one of possibilities.

For 3D case, we simulated short chains (up to $N = 700$). Our MC data indicate first-order result. The region of divergence of Binder cumulants and interval consisting of structural phase transition are approximately the same regions.

More work is needed to make more accurate predictions for phase transitions points.

Bibliography

[1] E.J.J. Van Rensburg. *The Statistical Mechanics of Interacting Walks, Polygons, Animals and Vesicles*. Oxford Lecture Series in Mathe. Oxford University Press, 2015. ISBN: 9780199666577. URL: https://books.google.ru/books?id=LIVMCAAAQBAJ.

[2] "Monte Carlo and Molecular Dynamics Simulations in Polymer Science Edited by Kurt Binder." In: (1995).

[3] Carlo Vanderzande. *Lattice models of polymers*. Cambridge University Press, 1998.

[4] "Statistical Physics". In: *Equilibrium Statistical Physics: Phases of Matter and Phase Transitions*. Ed. by Marc Baus and Carlos F. Tejero. Berlin, Heidelberg: Springer Berlin Heidelberg, 2008, pp. 45–63. ISBN: 978-3-540-74632-4. DOI: 10.1007/978-3-540-74632-4_3. URL: https://doi.org/10.1007/978-3-540-74632-4_3.

[5] Kit Fun Lau and Ken A Dill. "A lattice statistical mechanics model of the conformational and sequence spaces of proteins". In: *Macromolecules* 22.10 (1989), pp. 3986–3997.

[6] Jinfeng Zhang, S. C. Kou, and Jun S. Liu. "Biopolymer structure simulation and optimization via fragment regrowth Monte Carlo". In: *The Journal of Chemical Physics* 126.22 (2007), p. 225101. DOI: 10.1063/1.2736681. eprint: https://doi.org/10.1063/1.2736681. URL: https://doi.org/10.1063/1.2736681.

[7] Hsiao-Ping Hsu et al. "Growth-based optimization algorithm for lattice heteropolymers". In: *Phys. Rev. E* 68 (2 2003), p. 021113. DOI: 10.1103/PhysRevE.68.021113. URL: https://link.aps.org/doi/10.1103/PhysRevE.68.021113.

[8] Robert Helling et al. "The designability of protein structures". In: *Journal of Molecular Graphics and Modelling* 19.1 (2001), pp. 157 –167. ISSN: 1093-3263. DOI: https://doi.org/10.1016/S1093-3263(00)00137-6. URL: http://www.sciencedirect.com/science/article/pii/S1093326300001376.

[9] Kamilla Faizullina and Evgeni Burovski. "Globule-coil transition in the dynamic HP model". In: *Journal of Physics: Conference Series* 1740 (Jan. 2021), p. 012014. ISSN: 1742-6588. DOI: 10.1088/1742-6596/1740/1/012014.

[10] T Garel, H Orland, and E Orlandini. *Phase diagram of magnetic polymers*. 1999, pp. 261–268.

[11] Andrea Papale and Angelo Rosa. "The Ising model in swollen vs. compact polymers: Mean-field approach and computer simulations". In: *European Physical Journal E* 41 (12 Dec. 2018). ISSN: 1292895X. DOI: 10.1140/epje/i2018-11752-2.

[12] Damien Paul Foster and Debjyoti Majumdar. "Critical behavior of magnetic polymers in two and three dimensions". In: *Phys. Rev. E* 104 (2 2021), p. 024122. DOI: 10.1103/PhysRevE.104.024122. URL: https://link.aps.org/doi/10.1103/PhysRevE.104.024122.

[13] Kamilla Faizullina, Ilya Pchelintsev, and Evgeni Burovski. "Critical and geometric properties of magnetic polymers across the globule-coil transition". In: *Phys. Rev. E* 104 (5 2021), p. 054501. DOI: 10.1103/PhysRevE.104.054501. URL: https://link.aps.org/doi/10.1103/PhysRevE.104.054501.

[14] J M Kosterlitz and D J Thouless. "Ordering, metastability and phase transitions in two-dimensional systems". In: *Journal of Physics C: Solid State Physics* 6.7 (1973), pp. 1181–1203. DOI: 10.1088/0022-3719/6/7/010. URL: https://doi.org/10.1088/0022-3719/6/7/010.

[15] Martin Hasenbusch. "The two-dimensional XY model at the transition temperature: a high-precision Monte Carlo study". In: *Journal of Physics A: Mathematical and General* 38.26 (2005), 5869–5883. ISSN: 1361-6447. DOI: 10.1088/0305-4470/38/26/003. URL: http://dx.doi.org/10.1088/0305-4470/38/26/003.

[16] Marios Nikolaou. "A Matter of Disorder: Monte Carlo Simulations of Phase Transitions in Strongly Disordered Systems". PhD thesis. KTH, 2007.

[17] Kamilla Faizullina and Evgeni Burovski. "XY model on self-avoiding walks". Russian Supercomputing Days. Moscow, 2022. URL: https://russianscdays.org/en.

[18] Kurt Binder and Dieter W. Heermann. *Monte Carlo Methods for the Sampling of Free Energy Landscapes*. 2010, pp. 153–174. ISBN: 9783642031625. DOI: 10.1007/978-3-642-03163-2_6.

[19] Kurt Binder. "Finite size scaling analysis of Ising model block distribution functions". In: *Zeitschrift für Physik B Condensed Matter* 43.2 (1981), pp. 119–140.

[20] Bin Li, Neal Madras, and Alan D Sokal. *Critical Exponents, Hyperscaling, and Universal Amplitude Ratios for Two-and Three-Dimensional Self-Avoiding Walks*. 1995.

[21] Bertrand Duplantier and Hubert Saleur. *Exact Tricritical Exponents for Polymers at the e Point in Two Dimensions*. 1987.

[22] Paul J Flory. *Principles of polymer chemistry*. Cornell university press, 1953.

[23] Mark Newman and Gerard Barkema. *Monte Carlo methods in statistical physics chapter 1-4*. Oxford University Press: New York, USA, 1999.

[24] Nicholas Metropolis et al. "Equation of State Calculations by Fast Computing Machines". In: *The Journal of Chemical Physics* 21.6 (1953), pp. 1087–1092. DOI: 10.1063/1.1699114. eprint: https://doi.org/10.1063/1.1699114. URL: https://doi.org/10.1063/1.1699114.

[25] Sergio Caracciolo et al. "Geometrical properties of two-dimensional interacting self-avoiding walks at the θ-point". In: *Journal of Physics A: Mathematical and Theoretical* 44.11 (2011), pp. 1–24. ISSN: 17518113. DOI: 10.1088/1751-8113/44/11/115004. arXiv: 1012.1177.

[26] Alberto Berretti and Alan D Sokal. "New Monte Carlo method for the self-avoiding walk". In: *Journal of Statistical Physics* 40.3-4 (1985), pp. 483–531.

[27] Polidoros Paul Nidras. "Grand canonical simulations of the interacting self-avoiding walk model". In: *Journal of Physics A: Mathematical and General* 29.24 (1996), pp. 7929–7942. DOI: 10.1088/0305-4470/29/24/017. URL: https://doi.org/10.1088%2F0305-4470%2F29%2F24%2F017.

[28] Thomas Prellberg. "PERM and all that". Monte Carlo Algorithms in Statistical Physics. Melbourne, July 26-28. URL: https://webspace.maths.qmul.ac.uk/t.prellberg/talks/PERMandallthat.pdf.

[29] Peter Grassberger. "Pruned-enriched Rosenbluth method: Simulations of θ polymers of chain length up to 1 000 000". In: *Phys. Rev. E* 56 (3 1997), pp. 3682–3693. DOI: 10.1103/PhysRevE.56.3682. URL: https://link.aps.org/doi/10.1103/PhysRevE.56.3682.

[30] N. Prokof'ev and B. Svistunov. "Worm Algorithms for Classical Statistical Models". In: *Phys. Rev. Lett.* 87 (16 2001), p. 160601. DOI: 10.1103/PhysRevLett.87.160601. URL: https://link.aps.org/doi/10.1103/PhysRevLett.87.160601.

[31] Ulli Wolff. "Collective Monte Carlo Updating for Spin Systems". In: *Phys. Rev. Lett.* 62 (4 1989), pp. 361–364. DOI: 10.1103/PhysRevLett.62.361. URL: https://link.aps.org/doi/10.1103/PhysRevLett.62.361.

[32] Kamilla Faizullina. *Saw models*. https://github.com/kamilla0503/saw_models. 2022.

[33] P. S. Kostenetskiy, R. A. Chulkevich, and V. I. Kozyrev. "HPC Resources of the Higher School of Economics". In: *J. Phys.: Conf. Ser.* 1740 (2021), p. 012050. DOI: 10.1088/1742-6596/1740/1/012050. URL: https://doi.org/10.1088/1742-6596/1740/1/012050.

[34] Martin Hasenbusch. "The Binder cumulant at the Kosterlitz–Thouless transition". In: *Journal of Statistical Mechanics: Theory and Experiment* 2008.08 (2008), P08003. DOI: 10.1088/1742-5468/2008/08/p08003. URL: https://doi.org/10.1088%2F1742-5468%2F2008%2F08%2Fp08003.

[35] K. Binder and D. P. Landau. "Finite-size scaling at first-order phase transitions". In: *Phys. Rev. B* 30 (3 1984), pp. 1477–1485. DOI: 10.1103/PhysRevB.30.1477. URL: https://link.aps.org/doi/10.1103/PhysRevB.30.1477.